**The 14th International Topical Meeting on Nuclear Reactor Thermalhydraulics, NURETH-14**
**Toronto, Ontario, Canada, September 25-30, 2011**

**NURETH14-135**

# EXPERIMENTAL INVESTIGATION ON STEAM CONDENSATION IN THE PRESENCE OF AIR AND HELIUM: FORCED CONVECTION CONDITIONS

**M. Bucci[1,2], W. Ambrosini[1], N. Forgione[1], D. Lioce[1,3]**
[1] University of Pisa, DIMNP, Largo Lucio Lazzarino 2, 56126 Pisa, Italy
[2] CEA Saclay, CEA/DEN/DANS/DM2S/SFME/LETR, 91191 Gif-sur-Yvette, France
[3] Westinghouse Electric Belgium, Rue de l'Industrie 43, 1400 Nivelles, Belgium.
matteo.bucci@cea.fr

## Abstract

This paper discusses the results obtained from recent experimental investigations devoted to the study of steam condensation in the presence of air and a light noncondensable gas. The experiments are intended to provide data for the validation of engineering models and CFD codes. The original experimental data herein discussed focus on forced convection turbulent boundary layer conditions and involve atmospheric pressure, different conditions for mixture velocity (from 1.5 to 3.5 m/s), mixture composition (form 0 to 75 per cent of the light species in the overall amount of noncondensable gases) and two nominal electrical power supply of the steam generator. The experimental data are qualified against correlations based on the heat and mass transfer analogy and to the predictions obtained by an in house condensation model implemented in a commercial CFD code.

## 1. Introduction

Condensation in the presence of noncondensable gases has a well known relevance in nuclear safety analyses, since it represents an important heat sink for removing the energy released by the discharge of the primary water during a postulated loss of coolant accident. Nevertheless, it could strongly affect containment atmosphere mixing, influencing the distribution of hydrogen and other noncondensable gases hypothetically delivered in severe accident conditions.
Condensation in the presence of light noncondensable gases is therefore of primary relevance in safety analyses of the containment atmosphere, for which an in-depth understanding is desirable.
In the past decades the phenomenon has been investigated under the theoretical and the experimental point of view and extensive databases were made available by both integral and separate effect test facilities [1-16]. However, the need for producing new high quality experimental data has recently emerged to promote the validation of CFD codes in view of their application to containment safety analyses.
In this aim, the CONAN facility was set up some years ago at the University of Pisa, aiming at addressing steam condensation in the presence of air and helium in separate effect test conditions. Computational tools have been developed having multiple purposes. On one hand, mechanistic models based on the principles of diffusion have been developed and applied mainly to the analysis of small scale separate effect condensation tests [17,21,22]. These models, hardly applicable to large scale analysis are anyway useful to achieve a significant improvement in the understanding of physical phenomena involved in the condensation process. On the other hand, other models have been conceived purposed for the analysis of large scale facilities or full scale

containment [18-21]. These models have been developed based on the heat and mass transfer analogy or empirical and semi-empirical correlations.
In this paper the results of experimental campaigns performed within the CONAN facility are presented together with predictions obtained by a computational tool developed at UNIPI and implemented in the FLUENT code. The main features of the CONAN facility and its operation are firstly illustrated. Then, the method for the processing of experimental data is detailed. The analysis of available experimental data is therefore presented, accompanied by a description of the adopted CFD model and the results of computations.

## 2. The CONAN facility

The CONAN facility (CONdensation with Aerosols and Noncondensable gases) is operated by the Department of Mechanical, Nuclear and Production Engineering of the University of Pisa [22]. The apparatus was conceived to collect data of steam condensation of interest for nuclear reactor containment thermal-hydraulic analysis. The facility consists of three different loops, primary, secondary and tertiary (see Figure 1, left), which accomplish with the operating needs encountered in running the experiments:

- the primary loop, in which the mixture of steam and noncondensable gases circulates and partly condenses on a flat wall;
- the secondary loop, which provides the required cooling of the condensing plate by circulating water, whose temperature and flow rate can be varied;
- the tertiary loop, which allows controlling the temperature of the cooling fluid (the water of the secondary loop).

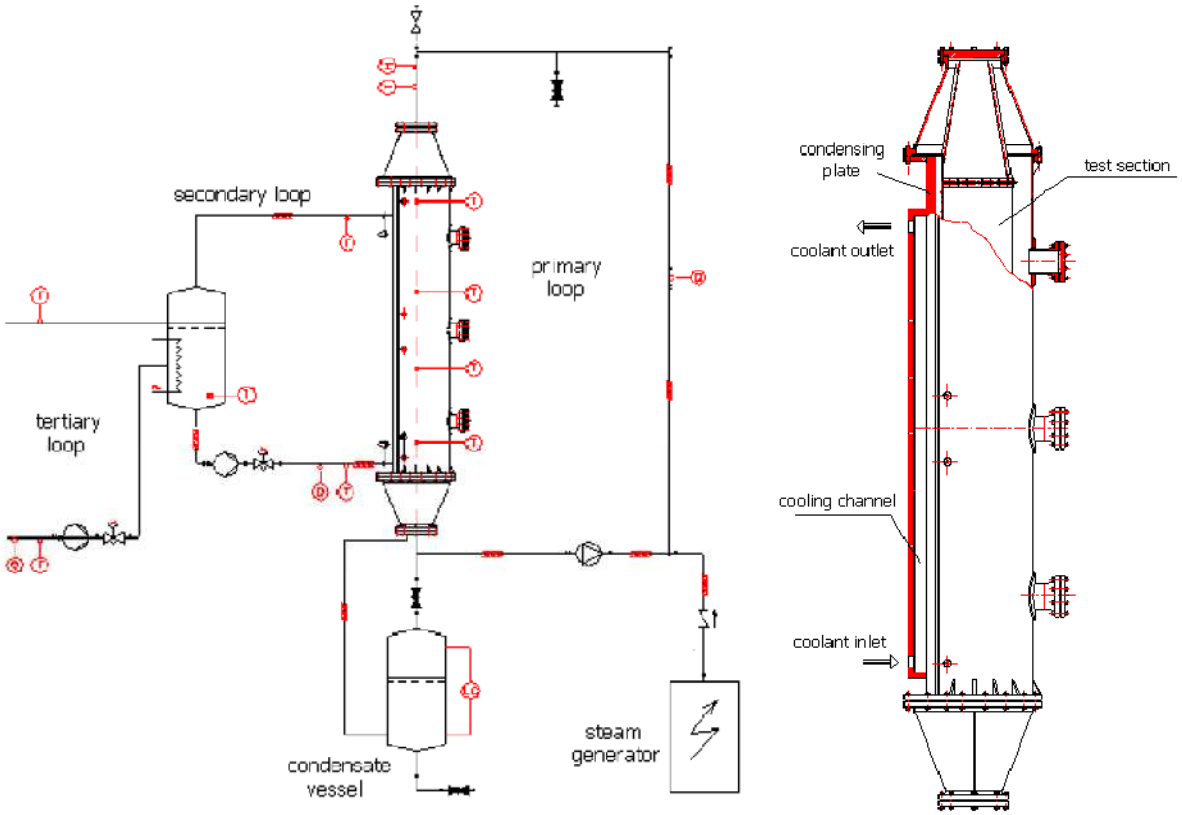


**Figure 1 Layout (left) and test section (right) of the CONAN facility.**

## 2.1 Main features of the CONAN facility

The primary loop contains the test section (see Figure 1, right), consisting in a roughly 2 m long, 0.34 m side channel having square cross section, in which a mixture of steam, air and helium is circulated. One of the lateral surfaces of the channel belongs to a 4.5 cm thick aluminium flat plate, cooled on the back side by the water of the secondary loop. Condensation occurs on the inner surface of the cooled plate and the related condensate flow is collected at its bottom by a gutter and routed by a small diameter piping to an external vessel; a relatively accurate estimate of the condensate flow is obtained by differential pressure measurement in this vessel. The other surfaces of the test section are kept reasonably insulated from the external environment, to avoid that condensation occurs over them. Variable area sections connect both the test section channel to the primary loop piping. The bottom part of the test section is connected to a variable speed blower for circulating the air-helium-steam mixture. Steam produced by a 60 kW electrical steam generator is injected at the bottom of the primary loop via a tee junction. The uppermost part of the primary loop is presently connected to the external atmosphere via an open pipe, to maintain atmospheric pressure conditions. The secondary loop includes a 5 mm deep, 35 cm wide rectangular cooling channel located on the back side of the aluminium plate, two collectors and pipes for routing water at the outlet of the cooling channel to a mixing vessel, being a component common to the secondary and tertiary loop. The vessel is equipped with three heaters, having each one a power of 3 kW, for water warming up during the start up phase and water temperature control during operation. A pump located at the exit of the mixing vessel routes extracted water again to the secondary channel. The tertiary loop has the role of extracting cold water from a large reservoir available on the site, pumping it into the mixing vessel and extracting by free fall into an outlet pipe an equal flow of warm water, thus obtaining the required power extraction from the secondary loop.

## 2.2 Operating procedure

In the tests performed up to now, at atmospheric pressure, the main operating variables are:

- the steam generator power, controlled by an electronic equipment manually operated in the facility control room;
- the primary volumetric flow, adjusted to the prescribed values by varying the frequency of the electrical supply of the blower motor through an inverter driven by the related computer software;
- the air-helium percentages, obtained by injecting helium in the primary circuit up to the desired concentration;
- the secondary coolant temperature at the inlet of the cooling channel, controlled by changing the tertiary loop flow and the temperature set point of the heaters in the mixing vessel;
- the secondary coolant flow rate.

Once the steam generator power and the primary flow are fixed and the secondary coolant flow and temperature are set to the prescribed values, the primary mixture temperature and concentration are automatically defined. In fact, starting with a mixture rich of noncondensable gases, injection of steam through the steam generator outlet line and spontaneous purging of the

excess noncondensable gases through the pipe open to the atmosphere increases steam concentration up to the point in which the obtained conditions allow a condensation rate equal to the inlet steam flow, provided this does not exceed the maximum system condensing capabilities. On the other hand, whenever the injected steam flow is lower than the condensation rate, the internal atmosphere tends to shrink, sucking air from the open pipe and decreasing the steam fraction down to a new equilibrium condition. Steady-state conditions can be therefore stably achieved, thus letting investigating a wide range of operating conditions.

Tests are labelled as P*aa*-T*bb*-V*cc*-H*ee*, where:

- *aa* is the nominal steam generator power in kW;
- *bb* is the nominal secondary coolant temperature at the inlet of the cooling channel [°C];
- *cc* is the nominal inlet velocity in decimal of m/s;
- *ee* is the nominal molar fractions of helium in the noncondensable gas.

In the following, the main steps of the operating procedure are summarized:

1. Heating up the water stored in the secondary loop. This is performed by three resistance heaters in the proper storage vessel. During this heating up phase, also the pump of this loop is running; the changes in the temperatures at the inlet and the outlet of the cooling section are measured and the temporal changes are displayed on the PC screen.
2. Activation of the primary circuit blower and the steam generator. This step aims at heating the primary circuit in order to minimize spurious condensation heat losses.
3. The flow rate is adjusted to achieve the desired inlet velocity in the test section.
4. The steam generator power is set to the desired operating value.
5. Filling of helium. The amount of helium is monitored to achieve the desired ratio with air and it is continuously measured during the course of the test.
6. The pump in the tertiary loop is activated and controlled, in order to evacuate from the secondary loop the heat released by condensation in the primary loop. The heaters in the mixing vessel compensate small unbalances.

Data coming from the measuring system are continuously acquired and monitored. Once steady-state conditions are reached, the available measures are recorded with a frequency of 0.5 Hz for periods of 600 seconds or more. The main measurements available in the facility are:

- temperature and relative humidity of the bulk mixture entering the test channel, estimated by temperature measurements through a dry bulb and a wet bulb thermal resistance, as indicated by Lioce [23];
- temperature of the bulk mixture at four locations along the channel, by calibrated K-type thermocouples;
- level in the condensate collecting tank, by which the condensation rate is deduced;
- volumetric flow of the mixture in the primary circuit, measured by a vortex flow meter;
- temperature at different locations and depths along and in the thickness of the aluminium plate, by 1 mm K-type thermocouples inserted in 1.1 mm holes drilled in the plate;
- temperature of the secondary coolant in the inlet and outlet collectors;
- flow rate of the secondary coolant, via a Coriolis type flow meter;
- temperature of the tertiary coolant at the inlet and at the outlet of the mixing vessel;
- pressure in the primary vessel;

- helium mole fraction, obtained by conductivity measurement of the noncondensable air-helium mixture, after sampling the mixture at the inlet of the channel and condensing the steam.

## 2.3 Data processing procedure

Several temperature measurements are available within the condensing plate, allowing to obtain the local heat flux values at 18 different points. Given the temperature values $TP_c$ and $TP_h$ measured on the condensing plate for a particular axial location at a distance x from the inlet section (see Figure 2), the corresponding transversal local heat flux Φ is given by:

$$\Phi = -k\frac{dT}{dy} = -k\frac{\Delta T}{e_p} = k\frac{TP_c - TP_h}{e_p}$$

where $k$ is the thermal conductivity of the plate, estimated at the average temperature $T_{avg}$, defined as:

$$T_{avg} = \frac{TP_c + TP_h}{2}$$

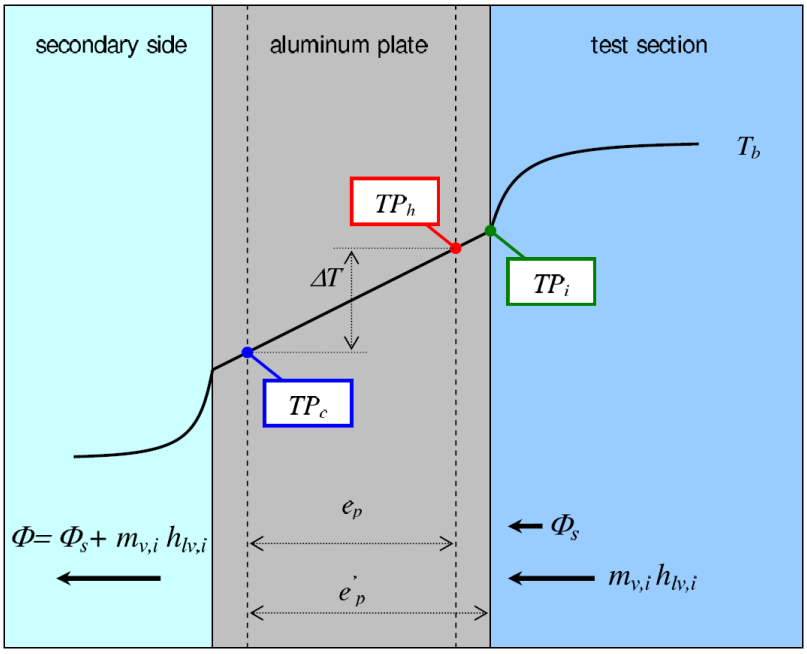


**Figure 2 Sketch of temperature profile within the condensing plate**

The temperature on the surface of the condensing wall $TP_i$ can be also estimated assuming a linear temperature profile across the aluminium plate:

$$TP_i = TP_c + (TP_h - TP_c)\frac{e'_p}{e_p}$$

Once the heat fluxes are known, to know the local mass fluxes it is necessary to separate the sensible heat transfer and the latent heat transfer contributions. If the assumption is done that the liquid film, if present, has negligible thickness and thus a negligible thermal resistance, the temperature at the condensing interface $T_i$ can be assumed equal to the temperature estimated on the condensing wall $TP_i$. As a consequence, it is:

$$\Phi = \underbrace{\Phi_s}_{sensible\ heat} + \underbrace{\dot{m}''_{v,i} h_{lv,i}}_{latent\ heat} \tag{1}$$

where $\Phi_s$ and $\dot{m}''_{v,i}$ are respectively the local sensible heat flux and the local condensation mass flux. Moreover, the ratio between the sensible heat flux and the condensation mass flux can be written as follows:

$$\frac{\Phi_s}{m_{v,i}} = \frac{h_s \Delta T}{h_m B_m} = \frac{\frac{Nu_x k}{x}(TP_i - T_b)}{\frac{Sh_x \rho D}{x}\left(\frac{Y_{v,i} - Y_{v,b}}{1 - Y_{v,i}}\right)} \tag{2}$$

where $Y_{v,i}$ is the local steam mass fraction at the interface and $Y_{v,b}$ is the steam mass fraction in the bulk. Here, the analogy between heat and mass transfer is introduced:

$$\frac{Nu_{0,x}}{Sh_{0,x}} = \left(\frac{Pr}{Sc}\right)^{\frac{1}{3}}$$

To extend the validity of the heat and mass transfer analogy to high condensation rates, the Stefan factor $F$ [24] and the Ackerman factor $A$ [25] are also introduced, defined as:

with

$$F = \frac{\phi_m}{e^{\phi_m} - 1} \qquad A = \frac{\phi_t}{e^{\phi_t} - 1}$$

$$\phi_m = \frac{\dot{m}''_{v,i}}{h_{m,0}} \qquad \phi_t = \frac{\dot{m}''_{v,i} C_{p,v,i}}{h_{s,0}}$$

Since it is reasonable to assume that $F \sim A$, the heat and mass transfer analogy can be turned to obtain:

$$\left(\frac{Pr}{Sc}\right)^{\frac{1}{3}} = \frac{Nu_{0,x}}{Sh_{0,x}} = \frac{Nu_x}{A}\frac{F}{Sh_x} \sim \frac{Nu_x}{Sh_x} \tag{3}$$

Substituting Eq.(3) in Eq.(2), after some mathematical manipulations, the ratio between average sensible heat flux and mass flux is given by:

$$\frac{\Phi_s}{m_{v,i}} = \frac{C_p\,(TP_i - T_b)}{\left(\frac{Y_{v,i} - Y_{v,b}}{1 - Y_{v,i}}\right)} \left(\frac{Sc}{Pr}\right)^{\frac{2}{3}} = \frac{C_p\,(TP_i - T_b)}{\left(\frac{Y_{v,i} - Y_{v,b}}{1 - Y_{v,i}}\right)} Le^{\frac{2}{3}} \tag{4}$$

The local sensible heat flux $\Phi_s$ and the local condensation mass flux $\dot{m}''_{v,i}$ are therefore obtained by solving simultaneously Eq.(1) and Eq.(4) . The experimental local Sherwood $Sh_x$ number can be finally calculated by:

$$Sh_x = \frac{\dot{m}''_{v,i} x}{\rho D_{vm}\, B_m} = \frac{\dot{m}''_{v,i} x}{\rho D_{vm}} \left(\frac{1 - Y_{v,i}}{Y_{v,i} - Y_{v,b}}\right)$$

The corrected local Sherwood $Sh_{0,x}$ number, deprived of suction effects, is instead given by:

$$Sh_{0,x} = \frac{\dot{m}''_{v,i} x}{\rho D_{vm}\, F\, B_m} = \frac{\dot{m}''_{v,i} x}{\rho D_{vm}} \left[\log\left(\frac{Y_{nc,b}}{Y_{nc,i}}\right)\right]^{-1} \tag{5}$$

Similarly, the local Nusselt $Nu_x$ number is given by:

$$Nu_x = \frac{\Phi_s\, x}{k\,(TP_i - T_b)}$$

All properties appearing in the definition of the Sherwood or the Nusselt number are defined as *film* properties and their value must be calculated according to the following rules:

$$\rho = \frac{\rho_i + \rho_b}{2} \quad D_{vm} = \frac{D_{vm,i} + D_{vm,b}}{2}$$
$$k = \frac{k_i + k_b}{2} \quad C_p = \frac{C_{p,i} + C_{p,b}}{2}$$

All these quantities are functions of the temperature at the condensing interface and the bulk temperature, as well as the mixture composition defined by the species molar fraction $X$. For this reason the *helium-to-noncondensable gas-ratio*:

$$\chi = \frac{X_{he}}{X_a + X_{he}}$$

must be know in the bulk and at the condensing interface. Whereas the value of $\chi$ is measured in bulk, the interface value must be hypothesized. Bucci et al. [26] showed that, due to convection and turbulence effects, in turbulent condensing boundary layers it can be assumed:

$$\chi_i \sim \chi_b$$

## 3. Analysis of experimental data

The test series considered in this paper include 18 tests. Two different nominal power levels of the steam generator (20 and 25 kW), five different mixture velocities (1.5, 2.0, 2.5, 3.0, and 3.5 m/s) and different helium concentration (from 0 to 75% of the total amount of noncondensable

gases) were considered. A useful way for analysing experimental results consists in comparing local experimental Sherwood numbers deduced by measurements, as shown in Eq.(5), to those predicted by the analogy adopting an appropriate correlation, which in turbulent forced convection could be predicted by the Schlichting's correlation [27]:

$$Sh_{0,x} = 0.0296\, Re_x^{0.8} Sc^{0.33} = 0.0296 \left(\frac{\rho\, V\, x}{\mu}\right)^{0.8} \left(\frac{\nu}{D_{vm}}\right)^{0.33}$$

In Figure 3 and Figure 4 the results of this analysis are shown for the series at 20 kW and 25 kW respectively. A remarkable agreement of experimental Sherwood number points and the Schlichting correlation is experienced for Reynolds number higher than $10^5$. As a conclusion, for fully developed forced convection condensation the heat and mass transfer analogy is capable of providing an appropriate description of phenomena.

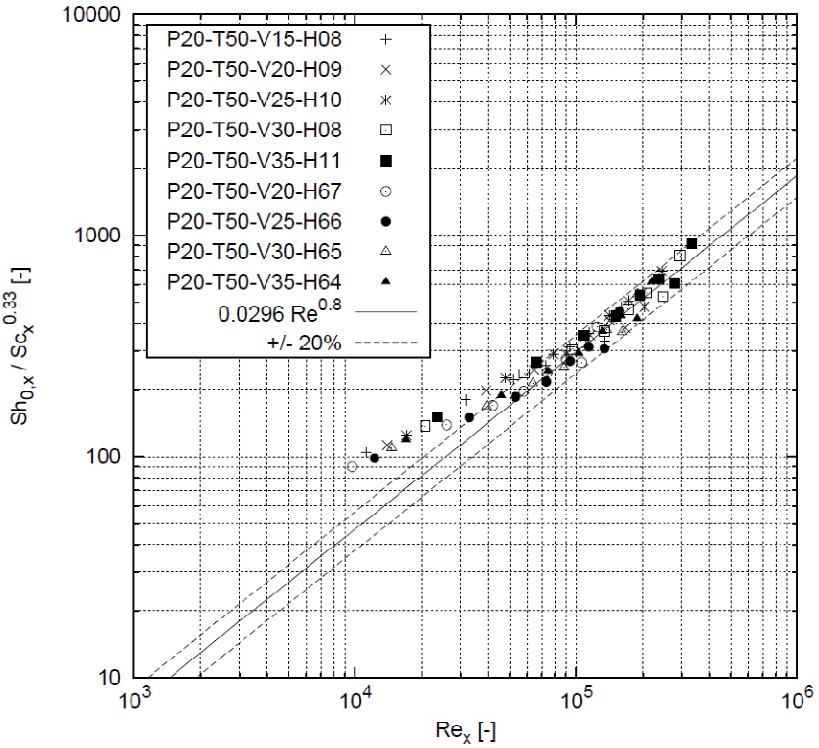


**Figure 3 Experimental Sherwood number in forced convection tests at 20 kW**

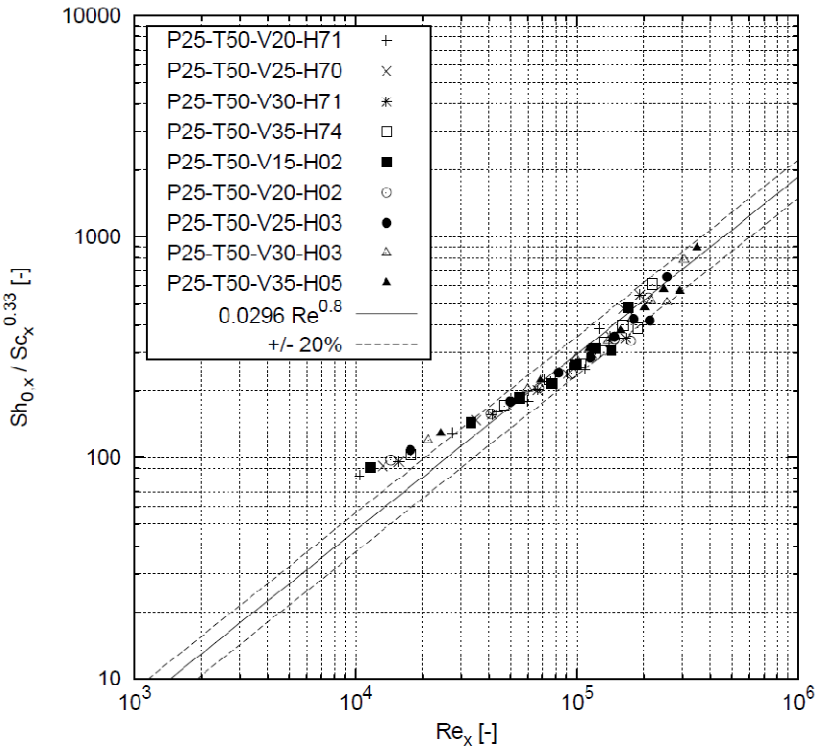


**Figure 4 Experimental Sherwood number in forced convection tests at 25 kW**

Relevant information provided by the analogy and confirmed by experiments is also that, for a given inlet velocity and a given steam generator power, helium concentration has a minor effect on the overall condensation rate (see Figure 5). The increase of the steam diffusivity and the condensation driving forces are in fact counterbalanced by a reduction of the mixture density, which implies a decrease of the maximum attainable Reynolds and Sherwood numbers. However, it can be shown that, for a given Reynolds number (and therefore a given Sherwood number), helium has a positive effect on the condensation rate (see the trends of experimental condensation rates for the two series at 20 and 25 kW in Figure 6): in this case density effects are limited and therefore the increase of molecular diffusivity results in an increase of the mass transfer coefficient and the of condensation rate.

## 3.1 Other formulation of the heat and mass transfer analogy

The various forms of the heat and mass transfer analogy can be roughly divided in two main categories: those cast in terms of mass fractions and therefore adopting a *mass approach* and those cast in terms of molar fraction, adopting a *molar approach*. In the present work, results available by the CONAN facility have been presented according to a formulation cast in terms of mass fraction, as reported in Spalding [29] or Lienhard [30]. However, in past studies, Ambrosini et al. [31] investigated the different forms of the heat and mass transfer analogy and quantified differences among the different formulations in the analysis of CONAN steam-air condensation tests.

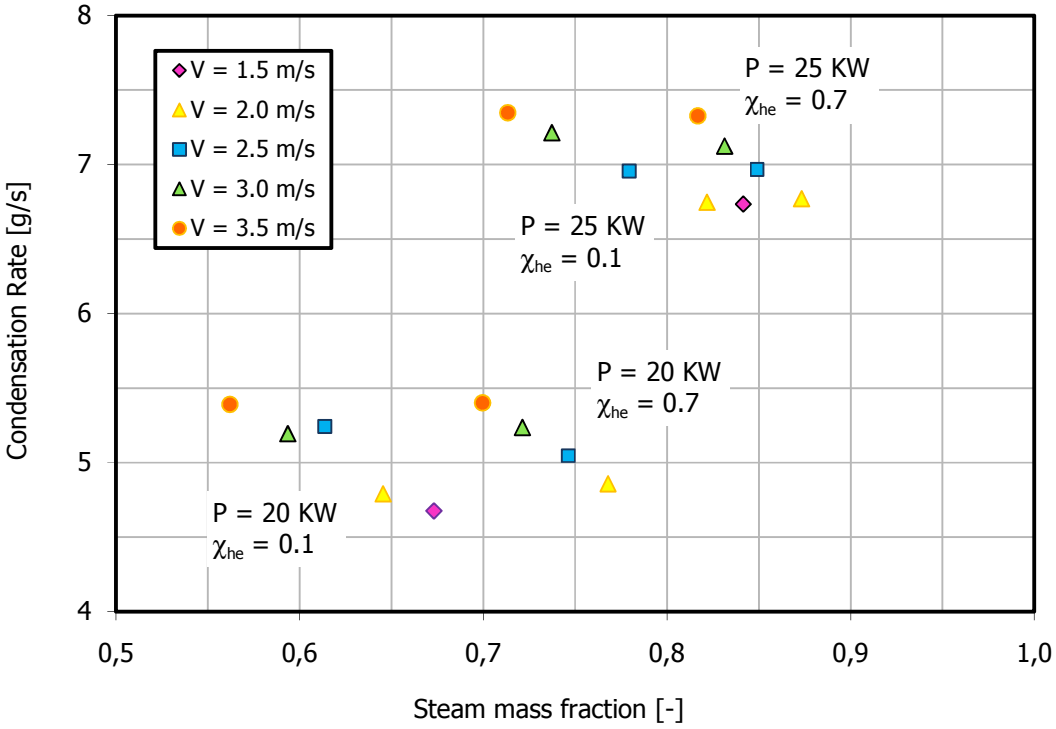


**Figure 5 Overall condensation rates vs. steam mass fractions**

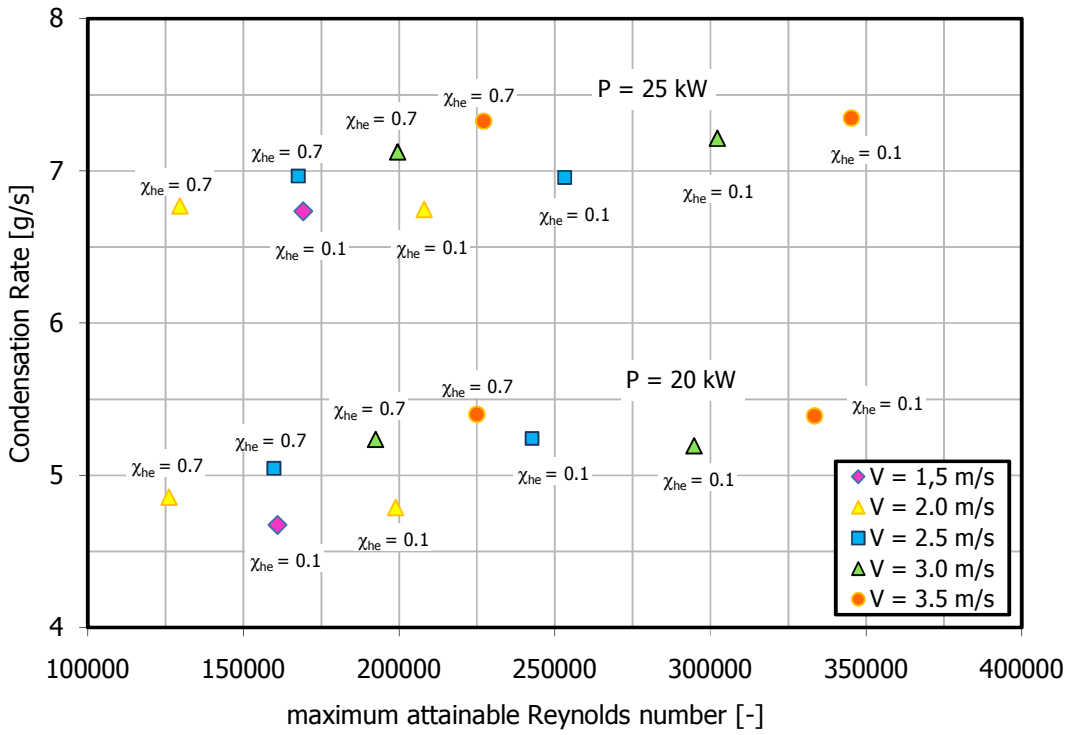


**Figure 6 Overall condensation rates vs. Maximum attainable Reynolds numbers**

In particular, they investigate the difference between the mass approach and the formulation of Bird [32], Chilton and Colburn [33], and Peterson et al. [34]. They showed that formulations based on the molar approach give higher Sherwood numbers with respect to the formulation based on the mass approach, but differences were relatively small (< 10%). In this section, the mass approach formulation is compared to the formulation of Bird and Peterson, for which the local Sherwood numbers are given respectively by:

$$Sh_{0,x,molar} = \frac{\dot{m}''_{v,i} x}{M_v \, c \, D_{vm}} \left[\log\left(\frac{X_{nc,b}}{X_{nc,i}}\right)\right]^{-1} \tag{6}$$

and

$$Sh_{0,x,Peterson} = \dot{m}''_{v,i} x \frac{h_{lv}}{k_c \left[T_i - T_{sat}(P_{v,b})\right]} \tag{7}$$

with

$$k_c = \frac{M_v^2 \, h_{lv}^2 \, P_0 D_{vm}^0}{\phi \, T_{avg} \, R^2 T_0^2} \quad \phi = -\frac{\log\left(\frac{1 - X_{nc,b}}{1 - X_{nc,i}}\right)}{\log\left(\frac{X_{nc,b}}{X_{nc,i}}\right)} \quad T_{avg} = \frac{T_b - T_i}{\log\left(\frac{T_b}{T_i}\right)}$$

For a given experimental mass flux $\dot{m}''_{v,i}$, the ratio between the Sherwood number predicted by the molar approach (6) and the mass approach (5) is given by

$$\frac{Sh_{0,x,molar}}{Sh_{0,x}} = \frac{M}{M_v} \frac{\log\left(\frac{X_{nc,b}}{X_{nc,i}} \frac{M_i}{M_b}\right)}{\log\left(\frac{X_{nc,b}}{X_{nc,i}}\right)} \tag{8}$$

where it was assumed that $\chi_i = \chi_b = \chi$, $M = \rho/c$ and

$$M_b = X_{v,b} M_v + (1 - X_{v,b})(\chi M_{he} + (1 - \chi) M_a)$$

$$M_i = X_{v,i} M_v + (1 - X_{v,i})(\chi M_{he} + (1 - \chi) M_a)$$

Differently from the case of binary mixture of steam and air, for which the ratio expressed by Eq.(8) is always greater than one, in steam-air-helium mixtures this ratio can be lower than unity. Indeed, depending on the helium concentration, the mixture molecular weight at the interface can be even lower than in bulk. In Figure 7, a comparison between the mass and the molar formulation is reported, together with the theoretical predictions obtained by Eq.(8), considering the average bulk and interface temperatures of the selected experimental series. As it can be deduced from Figure 7, when the interface mixture is heavier than the bulk mixture the molar approach tends to give higher Sherwood number values. On the contrary, if the interface mixture is lighter than the bulk, that is for high helium concentration in bulk, the molar approach predicts

lower values. The Peterson model is also compared to the mass formulation in Figure 8 Ratio of the Sherwood numbers calculated according to Peterson et al. [34] and Lienhard [30] models. Differently from the molar approach, for the available experimental data, the ratio between the Sherwood numbers in Eq.(7) and Eq.(5) is generally higher than unity. However, large differences could be experienced when the interface and bulk mixtures have similar molecular weight.

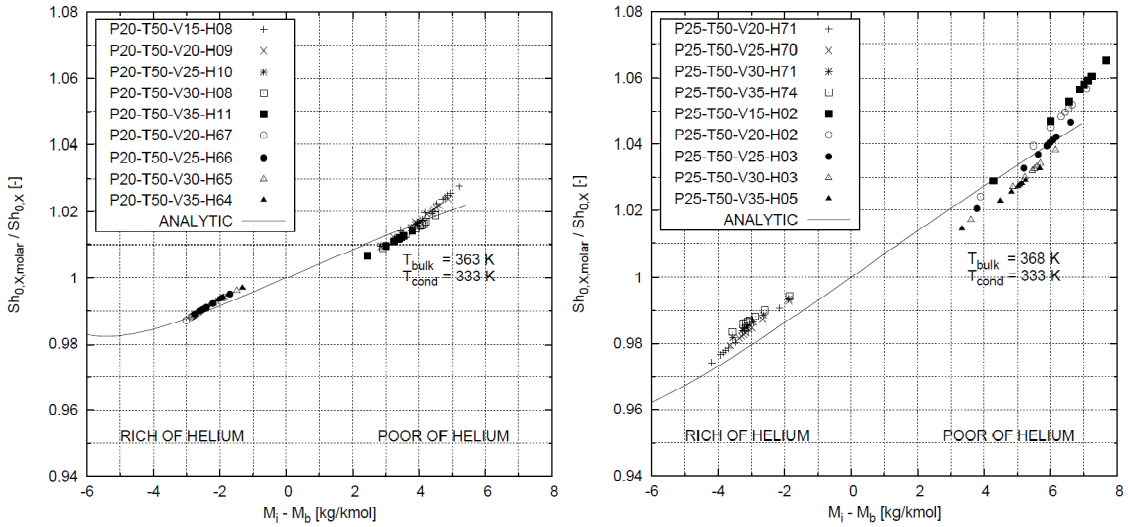


**Figure 7 Ratio of the Sherwood numbers calculated according to Bird et al. [32] and Lienhard [30] models.**

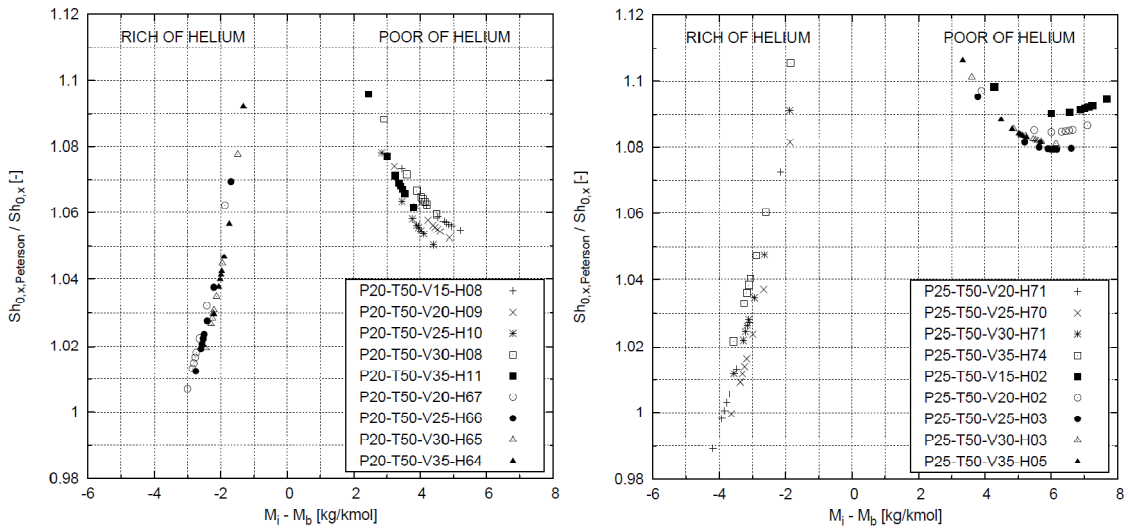


**Figure 8 Ratio of the Sherwood numbers calculated according to Peterson et al. [34] and Lienhard [30] models.**

## 4. Predictions by CFD tools

A common approach for modelling wall condensation in CFD codes consists on assigning volumetric source terms to cells adjacent to the condensing interface. These source terms are linked to the mixture continuity equation, the steam balance equation, the momentum and the energy balance equations. Volumetric sources of mass, steam, energy and momentum are therefore linked in the balance equations, respectively defined as

$$\textit{Overall Mass}\quad S_m = \dot{m}''_{v,i}/2\Delta c \qquad \textit{Steam}\quad S_v = S_m$$

$$\textit{Energy}\quad S_v = S_m h_{v,i} \qquad \textit{Momentum}\quad \mathbf{S_q} = S_m \mathbf{u}_c$$

where $2\Delta c$ is the thickness of the cell, $h_{v,i}$ is the steam enthalpy at the temperature of the condensing interface and $\mathbf{u}_c$ is the mixture velocity in the centre of the cell where the source term is applied. Moreover, the heat transfer through the condensing plate is modelled by the conjugated heat transfer approach by assigning an appropriate source term to the solid cells contiguous to the condensing interface

$$\textit{Energy in the solid plate}\quad S_{h,p} = -S_m h_{lv,i}$$

where $h_{lv,i}$ is the steam latent heat. In order to evaluate the condensation mass flux $\dot{m}''_{v,i}$ and thus the sources, different models have been developed adopting different strategies and having different purposes. These models are named HMTDM (Heat and Mass Transfer Diffusion Method) and HMTAM (Heat and Mass Transfer Analogy Method). Two different variants of the HMTDM model exist, depending on the diffusion method that they are based on: the effective binary diffusivity approximation (EBD) or the full multispecies mass transfer model (labelled MSD). Details of all these models are reported in [21] or [28]. In the next paragraph a summary description of the EBD model is given, whose capabilities in predicting condensation in the presence of air and helium are shown in section 4.3. Results obtained by the other models can be found in [21] or partially in [28].

### 4.1 The HMTDM model (Heat & Mass Transfer Diffusion Method)

The HMTDM model evaluates the mass transfer rates on the basis of concentration distributions in the near wall region, without requiring any specific closure law. It requires a very fine space meshing since its accuracy depends on the concentration profiles next to the condensing wall and therefore is hardly applicable to large scale geometries. It is anyway a very useful tool for achieving a better understanding of physical phenomena involved in condensation and relevant information for the development of coarser models for large scale analyses.
The condensation mass flux is calculated as

$$\dot{m}''_{v,i} = \frac{\mathbf{j}_{v,i} \cdot \mathbf{n}_i}{1 - Y_{v,i}}$$

where $\mathbf{j}_{v,i}$ is the steam diffusion mass flux at the interface and $\mathbf{n}_i$ is the normal to the condensing interface, pointing towards the fluid domain. The mechanistic character of the model consists in

the way the diffusion fluxes are calculated. According to the EBD approximation, the diffusion mass flux of a species is given by

$$\mathbf{j}_k = -\rho(D_{km} + D_t)\nabla Y_k$$

where the term $D_{km}$ is the equivalent binary diffusivity of the species *k* in the mixture and $D_t$ is the turbulent diffusivity, estimated according to the selected turbulence model. As shown in [26], this formulation provides an appropriate description of turbulent condensation phenomena in ternary mixtures. With respect to the MSD diffusion model that is due to provide a more accurate description of molecular transport effects, the EBD model is simpler to implement and is less expensive in terms of CPU time.
The turbulence model selected for this analysis is the RNG κ–ε. To deal with near wall turbulence, appropriate low Reynolds functions are adopted, which are referred to as Enhanced Wall Treatment in the FLUENT code [36].

### 4.2 Computational domain and boundary conditions

The optimized computational domain adopted for the modelling of CONAN tests with the FLUENT code is shown in Figure 9. The width of the fluid domain (0.34 m) is divided in 100 cells, refined near the walls according to the requirements of the turbulence model with low Reynolds capabilities; the nondimensional distance from the wall $y^+$ of the centre of cells adjacent to walls must be maintained lower than 1 for all tests. The fluid domain in front of the cooled plate is also divided in 100 longitudinal volumes. The region near the inlet section is more refined in order to provide a more detailed description of entrance effects. As shown in Figure 9, the fluid domain includes also the conical part near the outlet section, having adiabatic walls. Finally, the cooled plate (orange block in Figure 9) is discretized, having the same longitudinal discretization than the fluid domain and finely refined in the transversal direction.
At the inlet section, uniform temperature, concentration and velocity profiles are imposed. Turbulence intensity and equivalent hydraulic diameter are imposed as turbulence inlet conditions. On the secondary side of the condensing plate, a uniform heat transfer coefficient $h_{sec}$ is imposed with the cooling water of the secondary circuit, for which a linear temperature profile is assumed. To estimate $h_{sec}$ the Dittus-Boelter correlation for fully developed turbulent flows within pipes has been used.

### 4.3 Results of CFD analysis

The comparison between calculated and experimental values can be cast both in terms of integral and local quantities. In Figure 10, the overall condensation rates predicted by the EBD model are compared to the experimental ones. The behaviour of the model is excellent, mostly for the series at 25 kW, for which the discrepancy between calculated and experimental condensation rates never exceeds ±5% and the average discrepancy defined as

$$\sum_{i=1}^{n} \frac{\left|CR_{calc} - CR_{exp}\right|}{CR_{exp}}$$

is 2.57%. Tests at 20 kW are slightly underestimated, but the discrepancy never exceeds -15% and the average discrepancy is 7%, confirming the positive performance of the EBD model.

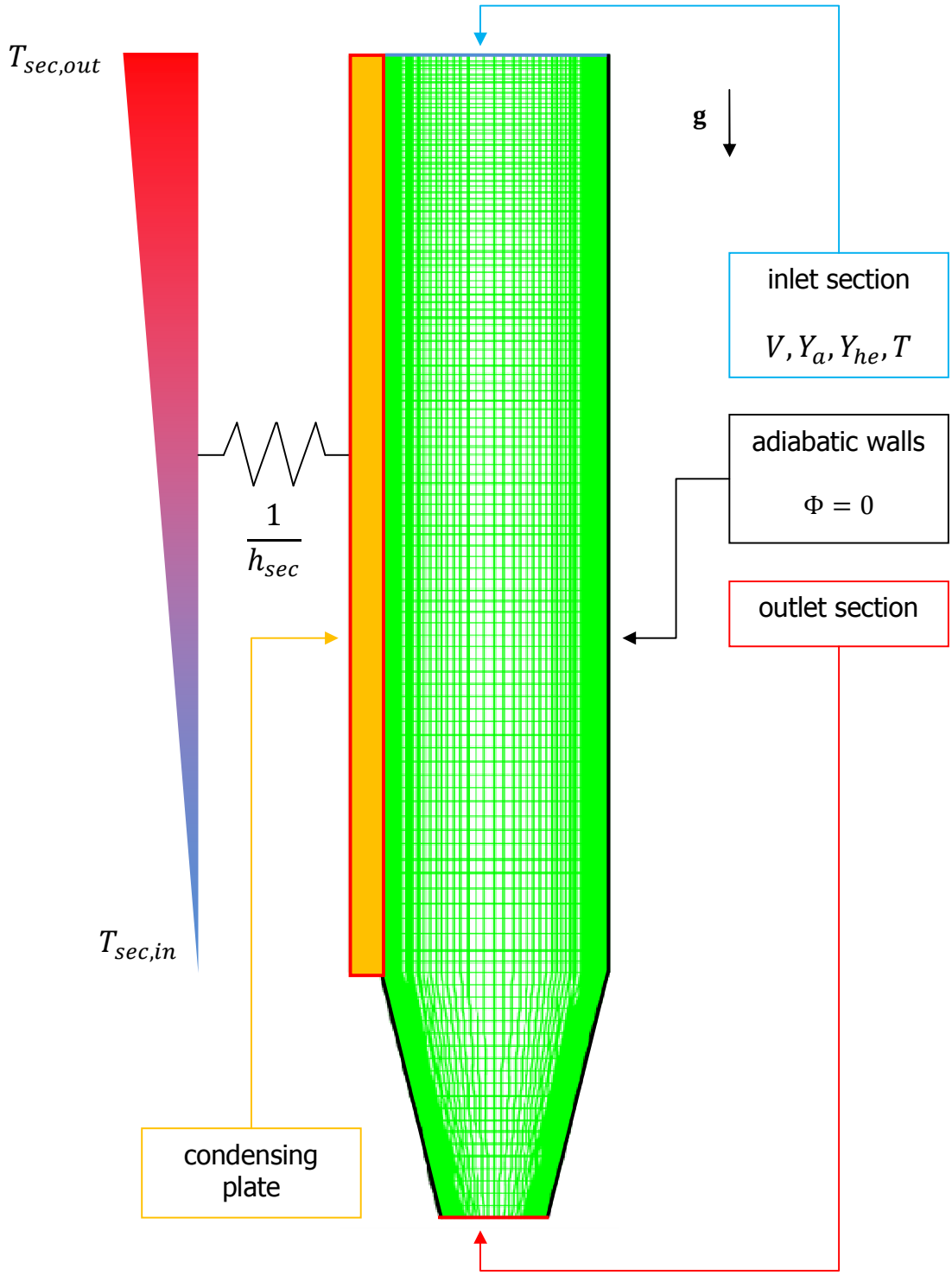


**Figure 9 Computational discretization and boundary conditions**

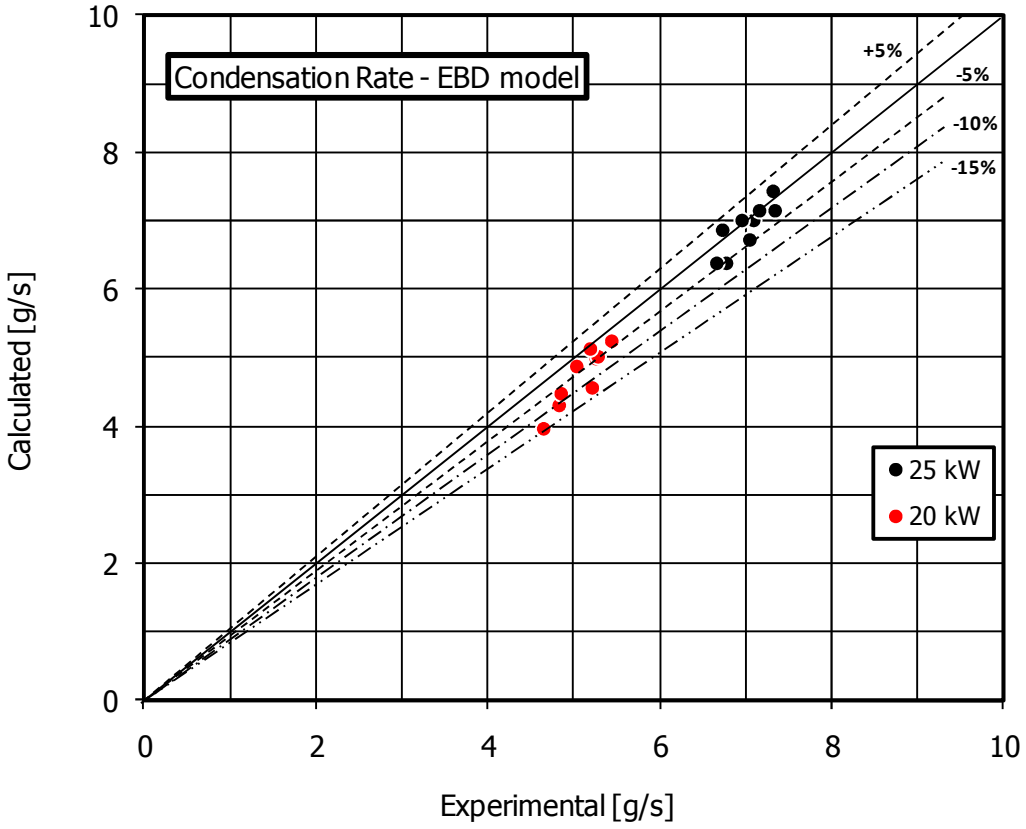


**Figure 10 Comparison between calculated and experimental condensation rates.**

In Figure 11 and Figure 12 the comparison between calculated and experimental local heat fluxes is shown for the two series. As it can be seen, the model is capable of providing an accurate description of the fully developed flow region in both series, where calculated heat fluxes are always included within the range of uncertainty of experimental measures. However, local heat fluxes and therefore local mass fluxes are slightly underestimated near the inlet section, resulting in a slight underestimation of the overall condensation rate, mostly for the series at 20 kW. Indeed, the selected turbulence model is capable of providing a satisfactory description of fully developed flow conditions, but lacks of accuracy in predicting developing boundary layers. This could be the reason for a slight underestimation of entrance effects. Entrance effects could be relevant also in the secondary circuit. A higher heat transfer coefficient should be expected in correspondence to the outlet section of the channel (the entrance region of the secondary channel) than the one based on the Dittus-Boelter correlation for fully developed flow conditions. As it can be seen in both figures, a slight increase of heat flux is in fact experienced in correspondence to the last thermocouples. Further improvements of aforementioned CFD models should take into account the developing length for the secondary heat transfer coefficient or even the modelling of the secondary circuit itself.

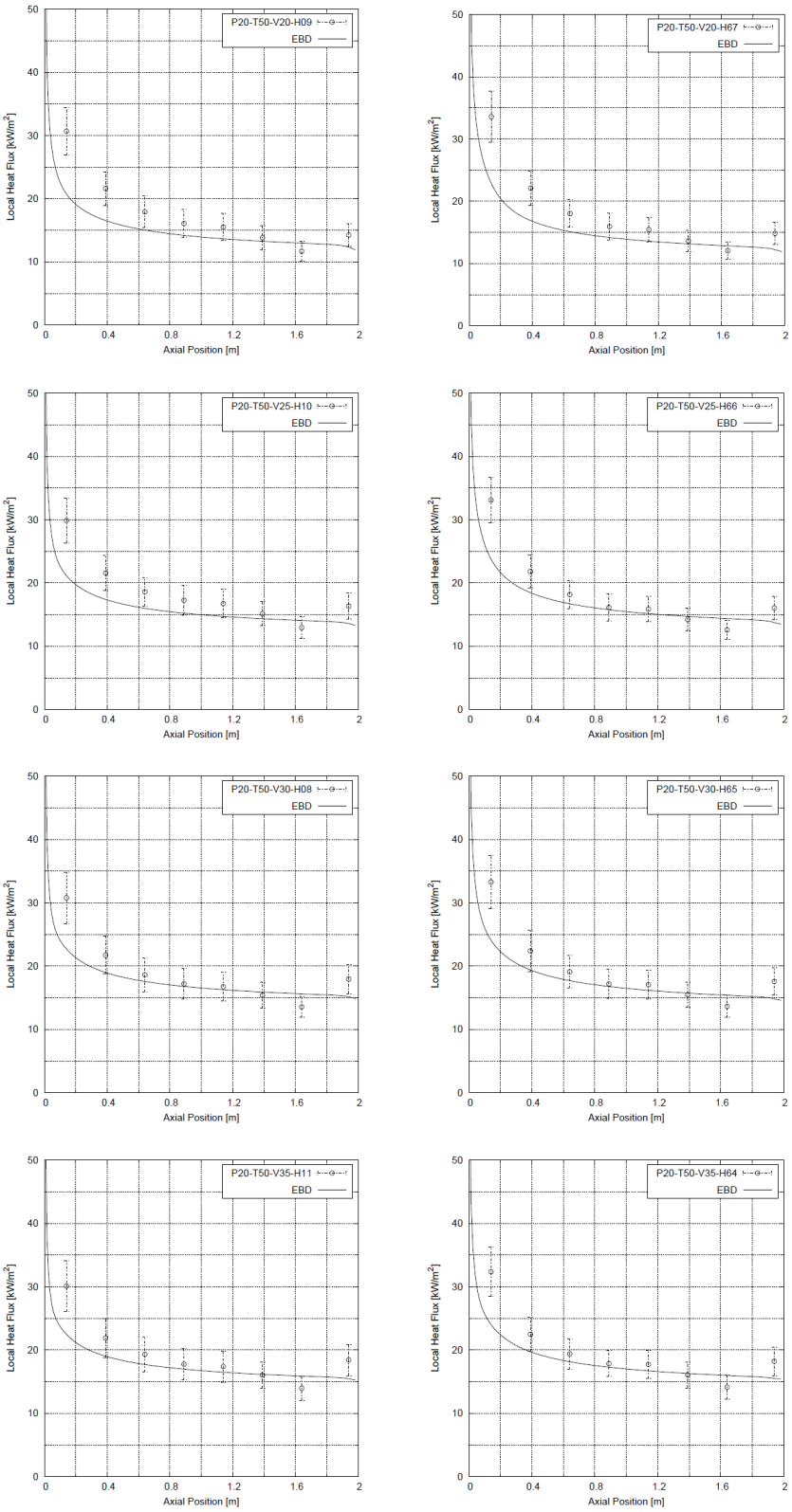


**Figure 11 Comparison between calculated and experimental heat fluxes in tests at 20 kW.**

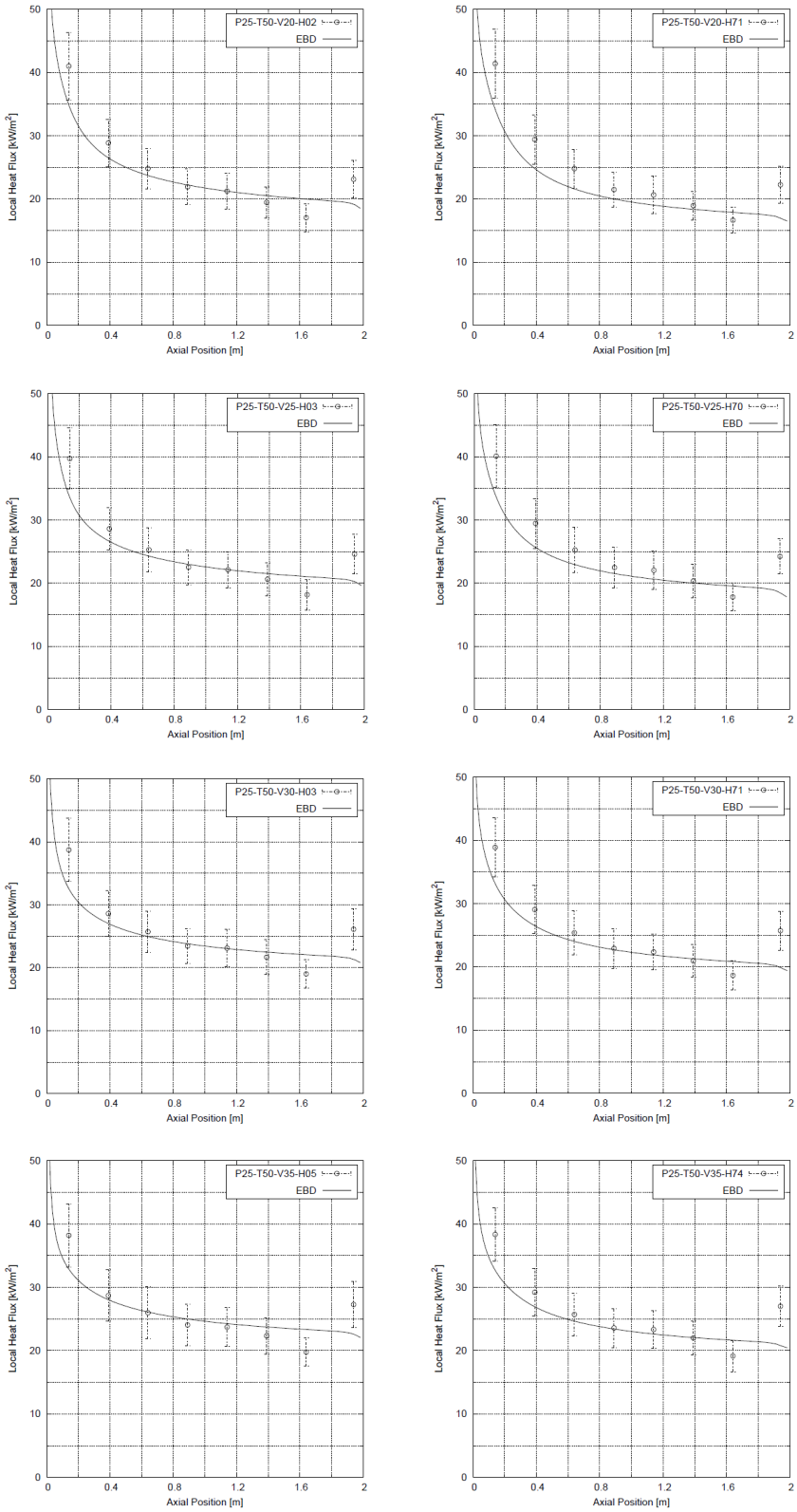


**Figure 12 Comparison between calculated and experimental heat fluxes in tests at 25 kW.**

## 5. Conclusion

This paper has presented the results of a recent experimental activity performed on condensation heat transfer in presence of air and helium. Forced convection turbulent boundary layer conditions have been addressed, varying the helium relative concentration from 0 to 75%. Experimental data have been qualified against the heat and mass transfer analogy and the prediction obtained by an in house CFD model named EBD used inside the Fluent code.
Sherwood numbers deduced from experimental measurements have been compared to estimations obtained by the heat and mass transfer analogy. Different formulations based both on the mass and the molar approaches have been adopted with the aim to improve the conclusions of a previous analysis proposed by some of the authors on the various forms of the analogy for steam-air mixtures [31]. The predictive character of the heat and mass transfer analogy has been clearly shown, demonstrating its capabilities in providing an appropriate description of the phenomenon.
Predictions obtained by the EBD condensation model have also been shown, demonstrating a very satisfactory behaviour of the model, mostly for fully developed flow regimes. Moreover, hints for future improvements in the modelling have been identified.

## 6. References

[1] K. Fischer, A.K. Rastogi, T. Braun, T. Drath, A. Lyubar, and S. Schwarz, “Containment code comparison exercise on experiment ThAI TH7”, Proceedings of the 10th International Topical Meeting on Nuclear Reactor Thermal Hydraulics (NURETH-10), Seoul, South Korea, 2003 October 5-9.

[2] H. J. Allelein, K. Fischer, J. Vendel, J. Malet, E. Studer, S. Schwarz, M. Houkema, H. Paillre, and A. Bentaib. „International standard problem ISP-47 on containment thermal-hydraulics”, Technical Report 10, OECD/NEA/CSNI, 2007.

[3] L. Blumenfeld and H. Paillère, “CFD simulation of mixed convection and condensation in a reactor containmetn: the MICOCO benchmark”, Proceedings of the 10th International Topical Meeting on Nuclear Reactor Thermal Hydraulics (NURETH-10), Seoul, South Korea, 2003 October 5-9.

[4] O. Auban, R. Zboray, and D. Paladino,”Investigation of large-scale mixing and stratification phenomena related to LWR containment studies in the PANDA facility”, Nuclear Engineering and Design, 237:409–419, 2007.

[5] A.A. Dehbi, ”The effects of noncondensable gases on steam condensation under turbulent natural convection conditions”, PhD thesis, Dept. of Nuclear Engineering, Massachusetts Institute of Technology, Cambridge, January 1991.

[6] I.K. Huhtiniemi, ”Condensation in the presence of a noncondensable gas: the effect of surface orientation”, PhD thesis, University of Winsconsin, 1991.

[7] I.K. Huhtiniemi and M.L. Corradini, ” Condensation in the presence of noncondensable gases”, Nuclear Engineering and Design, 141:429–446, 1993.

[8] A. Pernsteiner, I.K. Huhtiniemi, and M.L. Corradini, “Condensation in presence of noncondensable gases: effect of helium”, In Proceeding of the NURETH 6 conference, 1993.

[9] M.H. Anderson, L.E. Herranz, and M.L. Corradini, "Experimental analysis of heat transfer within the AP600 containment under postulated accident conditions",Nuclear Engineering and Design, 185:153–172, 1998.

[10] K.M. Vierow and V.E. Schrock, "An experimental investigation of the effect of air on steam condensation under turbulent natural convection, part.1 - heat transfer", In Proceeding of Int. Conf. on Multiphase Flow, Tsukuba, Japan, September 1991.

[11] D.G. Ogg, "Vertical downflow condensation heat transfer in gas-steam mixtures", Master's thesis, Dept. of Nuclear Engineering, University of California, Berkeley, January 1991.

[12] M. Siddique, "The effects of noncondensable gases on steam condensation under forced convection conditions",PhD thesis, Dept. of Nuclear Engineering, Massachusetts Institute of Technology, Canbridge, January 1991.

[13] M. Siddique, M. Golay, and M.S. Kazimi, "Local heat transfer coefficients for forced convection condensation of steam in a vertical tube in the presence of a noncondensable gas", Nuclear Technology, 102:386–401, 1993.

[14] S.Z. Kuhn, V.E. Schrock, and P.F. Peterson, "An investigation of condensation from steam-gas mixtures flowing downward inside a vertical tube", In Proceeding of the NURETH 7 conference, September 1995.

[15] S.Z. Kuhn, V.E. Schrock, and P.F. Peterson, "An investigation of condensation from steam-gas mixtures flowing downward inside a vertical tube", Nuclear Engineering and Design, 177:53–69, 1997.

[16] M.L. Corradini, "Turbulent condensation on a cold wall in the presence of a noncondensable gas", Heat Transfer and Fluid Flow, 64:186–195, February 1984.

[17] M. Bucci, M. Sharabi, W. Ambrosini, N. Forgione, F. Oriolo, and S. He, "Prediction of tranpiration effects on heat and mass transfer by different turbulence models", Nuclear Engineering and Design, 38:958–974, 2008.

[18] M. Bucci, E. Studer, J.P. Magnaud and W. Ambrosini, "Modelling of steam condensation phenomena in the presence of noncondensable gases: analysis of separate effect tests in forced, natural and mixed convection", Proceeding of the NURETH 13 conference, Kanazawa City, Ishikawa Prefecture, Japan, September 27 - October 2 2009.

[19] M. Bucci, W. Ambrosini, N. Forgione, F. Oriolo, and S. Paci, "Validation of a CFD condensation model based on the heat and mass transfer analogy by TOSQAN facility ISP47 test", In Proceeding of the ICONE 14 conference, Miami, Florida, July 17-20 2006.

[20] M. Bucci**, "**Sviluppo di modelli di CFD per lo studio della condensazione nel sistema di contenimento di LWRs**",** Master's thesis, University of Pisa, 2005.

[21] M. Bucci, "Experimental and computational analysis of condensation phenomena for the thermal-hydraulic analysis of LWRs containments", PhD Thesis, University of Pisa, 2009 June 19th.

[22] W. Ambrosini, N. Forgione and F. Oriolo, "Experimental and CFD analysis on condensation heat transfer ina square cross section channel", Proceedings of the 11th International Topical Meeting on Nuclear Reactor Thermal Hydraulics (NURETH-11), Avignon, France, 2006 October 2-6.

[23] D. Lioce, "Prove di condensazione di miscele ternarie di aria-elio-vapore e qualifica mediante un codice di CFD", MSc Thesis, University of Pisa, 2006.

[24] J. Stefan, "Versuche über die verdampfung", Sber. Akad. Wiss. Wien., 68:385-423, 1873.

[25] G. Ackermann, "Wäemeübertregung und molekulare stoffübertragung in gleichen feld bei grosser temperature und partialdruckdifferenzen", ForscHft. Ver. Dt. Ing., 328:1-16, 1937.

[26] M. Bucci, W. Ambrosini, and E. Studer, "Theoretical and computational analysis of diffusion phenomena in condensing multicomponent mixtures", *Submitted to* Nuclear Engineering and Design, 2010.

[27] H. Schlichting and K. Gersten, "Boundary layer theory", Springer-Verlag, Berlin, 8th edition, 2000.

[28] M. Bucci, W. Ambrosini, N. Forgione, F. Oriolo and S. Paci, "Experimental and computational analysis of steam condensation in the presence of air and helium", Proceedings of the 14th International Topical Meeting on Nuclear Reactor Thermal Hydraulics (NURETH-14), Toronto, Ontario, Canada, 2011 September 25-29.

[29] D.B. Spalding, "A standard formulation of the steady convective mass transfer problem", International Journal of Heat and Mass Transfer, 1:192-207, 1600.

[30] J.H. Lienhard, "A Heat Transfer Textbook", Prentice Hall, Englewood Cliffs, 1997.

[31] W. Ambrosini, N. Forgione, A. Manfredini, and F. Oriolo, "On various forms of the heat and mass transfer analogy: Discussion and application to condensation experiments", Nuclear Engineering and Design, 236:1013-1027, 2010.

[32] R. Bird, W.E. Stewart, and E.N. Lightfoot, "Transport Phenomena", Wiley, New York, 1960.

[33] T.H. Chilton and A.P. Colburn, "Evaporation of water into a laminar stream of air and superheated steam", Ind. Eng. Chem., 26:373-380, 1934.

[34] P.F. Peterson, V.E. Schrock, and T. Kageyama, "Diffusion layer theory for turbulent vapor condensation with noncondensable gases", Journal of Heat Transfer, 115:998-1003, 1993.

[35] R. Taylor and R. Kristhna, "Multicomponent Mass Transfer", Wiley, 1993.

[36] Fluent Inc.,"Fluent 6.2 user guide", Centerra Resource Park, Lebanon, NH., 2003.